Title

Solution-processable copper(I) iodide-based inorganic-organic hybrid semiconductors composed of both coordinate and ionic bonds

Authors

Hei, Xiuze

Zhu, Kun

Carignan, Gia

et al.

Publication Date

2022-10-01

DOI

10.1016/j.jssc.2022.123427

Solution-processable copper(I) iodide-based inorganic-organic hybrid semiconductors composed of both coordinate and ionic bonds

Xiuze Hei, [a, +] Kun Zhu, [a, +] Gia Carignan, [a] Simon J. Teat, [b] Mingxing Li, [c] Guoyu Zhang, [a] Megan Bonite [a] and Jing Li*, [a]

[*] Corresponding author

[a] Department of Chemistry and Chemical Biology, Rutgers University, Piscataway, NJ 08854, USA

Email: jingli@rutgers.edu

[b] Advanced Light Source, Lawrence Berkeley National Laboratory, Berkeley, CA 94720, USA

[c] Center for Functional Nanomaterials, Brookhaven National Laboratory, Upton, NY 11973, USA

[+] Equal contributions

Abstract

Three new one-dimensional (1D) All-In-One (AIO) type CuI-based hybrid semiconductors with both dative and ionic bonds between the inorganic and organic components have been successfully designed and synthesized by using the ligands containing both cationic center and coordination available sites. Structural analysis confirms that all compounds share the same formula of $Cu_4I_6(L)_2$ (L = ligand) and are composed of 1D-$Cu_4I_6^{2-}$

anionic chains that coordinate to cationic ligands. These materials demonstrate high stability towards heat and moisture and excellent solution processability due to their unique bonding nature. They emit low energy light ranging from green to orange color (530-590 nm). The origin and mechanism of their emissions were studied by both experimental and theoretical methods. More importantly, all compounds can be easily fabricated into films by solution process, a desired but rare feature for most of CuI-based hybrids built of extended networks.

Introduction

Crystalline hybrid metal halide semiconductor materials possess a wide range of interesting properties that are not only adopted from the individual inorganic and organic motifs, but also resulted from the interplay of the two components.[1-4] These hybrid materials are of great interest due to their potential in clean energy related applications, including solar cells,[5] light-emitting diodes,[6, 7] photocatalysis,[8, 9] and lasing.[10] Given different combinations of metal halides and organic ligands, their structures can vary from low dimensional molecular (0D) clusters to extended networks (1D-3D) with different metal coordination environments.[11-13] Octahedrally or tetrahedrally coordinated metal ions are often observed in the case of transition metal halide hybrid materials, examples including Ag-,[14] Mn-,[15] and Cu-based[16-18] systems.

Copper(I) iodide-based hybrid materials are of particular interest for photoluminescence related applications due to their well-known features including excellent optical properties, non-toxicity, facile synthesis, and structural diversity.[19-21] Those composed of Cu(I)-ligand coordinate bonds possess remarkable luminescent tunability, originated from their diverse emission mechanisms, namely, metal halide-to-ligand charge transfer [(M+X)LCT] and cluster-centered (CC) emissions.[22, 23] Therefore, their emission energies can be finely

tuned by adjusting the lowest unoccupied molecular orbital (LUMO) energy level of the organic ligands or altering the structure of the inorganic motifs.[19, 24] Based on the bonding nature between the inorganic and organic motifs, the existing CuI-based hybrid materials can be divided into three types. In type I structures, both inorganic CuI modules and organic ligands are charge-neutral and they form coordinate bonds.[25, 26] Type II structures are composed of cationic ligands and anionic inorganic modules, which form pure ionic bonds. [27-29] While applaudable progress has been made in the past decades on the design and optimization of these two types of CuI-based hybrid materials for general lighting applications, limitations still exist. Type I compounds of extended networks can be designed to give intense photoluminescence (PL) and optical tunability, but they suffer from poor solution processability. On the other hand, type II compounds, which are more soluble, usually manifest limited structural tunability and large stokes shifts. To overcome the above disadvantages, introducing both ionic bonds (as in type II compounds) and dative bonds (as in type I compounds) between the inorganic and organic motifs gives rise to a new structure type (Type III), denoted as AIO-type structures.[22, 30-32] Due to unique bonding characteristics, AIO-type structures inherit all the beneficial features of type I (e.g. facile tunability, intensive PL) and type II (e.g. high solution processability, stability), and thus, demonstrate great promise for solution-processed fabrication of low-cost thin-film devices, which would be difficult for both type I and type II compounds.[4, 7, 23, 24]

Herein, we report three new 1D-AIO structures that composed of 1D-Cu_4I_6 inorganic chains, namely, 1D-Cu_4I_6(*bttmm*)$_2$ (**1**, *bttmm* = 1-(1H-benzo[d][1,2,3]triazol-1-yl)-*N,N,N*-trimethylmethanaminium), 1D-Cu_4I_6(*mmtp*)$_2$ (**2**, *mmtp* = 1-methyl-4-(methylthio)pyridin-1-ium), and 1D-Cu_4I_6(*btmmp*)$_2$ (**3**, *btmmp* = 3-((1H-benzo[d][1,2,3]triazol-1-yl)methyl)-1-methylpyridin-1-ium). Two different inorganic backbones and ligand binding modes are

found in these structures. The photophysical properties, emission mechanisms and electronic structures of these compounds are examined by both experimental and theoretical methods. All compounds remain stable up to 210 °C and emit light in the green to orange region (530-590 nm) under UV irradiation. Notably, all compounds are highly soluble in DMSO despite the infinite nature of the inorganic chains, making the facile thin-film fabrication possible.

Experimental Section

Materials

Copper iodide (98%, Alfa Aesar); 1H-benzo [1,2,3]-triazole (99%, Alfa Aesar); potassium iodide (99%, Alfa Aesar); potassium carbonate (99%, TCI); acetonitrile (99.5%, VWR); methanol (99%, Alfa Aesar); dimethyl sulfoxide (99%, Alfa Aesar); 3-(Chloromethyl)pyridine hydrochloride (98%, TCI); Iodomethane (99%, Alfa Aesar); Formaldehyde (37% in aqueous solution, Alfa Aesar); Thionyl chloride (99%, Alfa Aesar); Trimethylamine (33% in ethanol, Alfa Aesar); 4-Mercaptopyridine (97%, TCI) and sodium salicylate (99%, Merck).

Preparation of 1-(1H-benzo[d][1,2,3]triazol-1-yl)-*N,N,N*-trimethylmethanaminium iodide *(bttmm)*

1-(Chloromethyl)-1H-benzo[d][1,2,3]triazole (*Cl-mbt*) was prepared according to the reported procedures.[30] In a round bottom flask, *Cl-mbt* (3.8 g, 25 mmol), acetone (20 ml) and KI (5 g) were charged and stirred for 4 hours before the solution was filtered. The filtrate was evaporated under reduced pressure and then added with trimethyl amine and acetonitrile (100 ml). After stirring under 65 °C for 3 days, the reaction mixture was evaporated under

reduced pressure and washed with ethyl ether to yield light brown solid. Drying under vacuum and recrystallized with ethanol gives white solid as final product. The yield is 57%.

Preparation of 1-methyl-4-(methylthio)pyridin-1-ium iodide *(mmtp)*

In a round-bottom flask, 4-Mercaptopyridine (1.12 g, 10 mmol), K_2CO_3 (20 mmol), and DCM (30 ml) were added and stirred for 10 min at 0 °C. Then iodomethane (1.7 g, 12 mmol) was added, followed by Et_3N (1 ml). After stirring overnight at room temperature, the reaction mixture was extracted with DCM, dried, and purified by chromatography to give yellow liquid, 4-(methylthio)pyridine (*mtp*). Iodomethane (1.13 g, 8 mmol) and *mtp* (556 mg, 5 mmol) were dissolved in MeCN (30 ml) and stirred overnight at room temperature. Then the reaction mixture was evaporated under reduced pressure and washed with ethyl ether. Recrystallization with ethanol gives pale yellow solid as final product. The yield is 70%.

Preparation of 3-((1H-benzo[d][1,2,3]triazol-1-yl)methyl)-1-methylpyridin-1-ium iodide *(btmmp)*

3-(Chloromethyl)pyridine hydrochloride (1.6 g, 10 mmol), K_2CO_3 (20 mmol), were added to a solution of benzotriazole (1.2 g, 10 mmol) in MeCN (100 ml) and were refluxed under stirring for 1 day. After cooling to room temperature, the reaction mixture was filtered. The filtrate was evaporated under reduced pressure and then purified by column chromatography, giving white solid, 1-(Pyridin-3-ylmethyl)-1H-1,2,3-benzotriazole (*pmbt*). Iodomethane (1.13 g, 8 mmol) and *pmbt* (1.05 g, 5 mmol) were dissolved in MeCN and stirred at room temperature overnight. After removal of MeCN under reduced pressure and washing with ethyl ether, the crude product was recrystallized with ethanol to give white powder as final product. The yield is 72%.

Synthesis of 1D-Cu_4I_6(*bttmm*)$_2$ (1)

CuI (38 mg, 0.2 mmol) was dissolved in KI saturated aqueous solution (2 ml) in a reaction vial. Acetonitrile (2 ml) was added as another layer followed by the slow addition of the ligand *bttmm* (33 mg, 0.1 mmol) in methanol solution (2 ml). The reaction mixture was kept undisturbed at 60 °C for 3 days. Block-like yellow single crystals, along with crystalline powder, were collected after filtration. The yield is 70%.

Synthesis of 1D-Cu_4I_6(*mmtp*)$_2$ (2)

A solution of CuI (57 mg, 0.3 mmol) in KI saturated aqueous solution (2 ml), MeCN (2 ml) and the solution of *mmtp* (27 mg, 0.1 mmol) in methanol (2 ml) were added in sequence into a vial and placed in 60 °C oven for 3 days. Rod-like yellow crystals were collected after filtration. The yield is 49%.

Synthesis of 1D-Cu_4I_6(*btmmp*)$_2$ (3)

Compound **3** was synthesized in the same way as that of compound **1** using *btmmp* as ligand. Needle-like yellow crystals were collected in 3 days. The yield is 65%.

Film Fabrication

Precursor solutions were made by dissolving compound **1** (100 mg) in DMSO (1 ml) under sonication and filtered through a PTFE filter (0.45 μm) before one-step drop-casting on precleaned glass substrates. This was followed by annealing at 110 °C in the glove box for 30 min.

Single crystal X-ray diffraction (SCXRD)

Single crystal data were collected using a D8 goniostat equipped with a Bruker PHOTON100 CMOS detector at the Advanced Light Source (ALS), Lawrence Berkeley National Laboratory, using synchrotron radiation. The structures were solved by direct methods and refined by full-matrix least-squares on F^2 using the Bruker SHELXTL package. [33] The structures were deposited in Cambridge Crystallographic Data Centre (CCDC) with numbers 1943657, 1498475 and 2167563.

Powder X-ray diffraction (PXRD) analysis

Powder X-ray diffraction (PXRD) analysis was carried out on a Rigaku Ultima-IV unit using Cu $K\alpha_1$ radiation (λ = 1.5406 Å). The operation power was 40 kV/44 mA. Data were collected in a 2θ range of 3 – 35 ° with a scan speed of 2 °/min.

Thermogravimetric analysis (TGA)

Thermogravimetric analyses (TGA) of samples were performed using the TA Instrument Q5000IR thermogravimetric analyzer with nitrogen flow and sample purge rates at 10 and 25 ml/min, respectively. About 5 mg of the samples were heated from room temperature to 500 °C at a rate of 10 °C/min under the nitrogen flow.

Photoluminescence measurements

Room temperature PL measurements were carried out on a Horiba Duetta fluorescence spectrophotometer at room temperature. Excitation spectra were measured and monitored at the emission wavelength of maximum intensity. Powder samples were evenly distributed and sandwiched between two glass slides.

Temperature dependent PL spectra and time-resolved PL decays were recorded on a home-built time-correlated single photon counting instrument. The PL signals were acquired using an average power of 0.55 mW, with decays recorded in at least 1000 channels using a 532 nm long path filter. PL decays were individually fit with the Fluofit Picoquant software using biexponential fit model.

Diffuse reflectance spectroscopy

Diffuse reflectance spectra were recorded on a Shimadzu UV-3600 UV-Vis-NIR spectrometer at room temperature. The reflectance was converted to Kubelka-Munk function, $\alpha/S = (1-R)^2/2R$ (α is the absorption coefficient, R is the reflectance and S is the scattering coefficient. S was treated as a constant since the average particle size of samples is significantly larger than 5 μm).

Internal quantum yield (IQY) measurements

IQYs were recorded using a C9920-02 absolute quantum yield measurement system (Hamamatsu Photonics) with a 150 W Xenon monochromatic light source and 3.3-inch integrating sphere. Sodium salicylate was used as the standard with a reported IQY of 60%.

DFT calculations

The density of states of selected compounds was calculated using the Cambridge Serial Total Energy Package (CASTEP) in Materials studio package using the crystal structures obtained from single-crystal X-ray analysis. Generalized gradient approximations (GGA) with Perdew-Burke-Ernzerhof (PBE) exchange correlation functional (XC) were used for all calculations. The plane-wave kinetic energy cutoff was set as 351 eV, ultrasoft

pseudopotentials were used for all chemical elements and the total energy tolerance was set to be 1×10^{-5} eV/atom.

Results and Discussion

All 1D-AIO structures contain 1D anionic $Cu_4I_6^{2-}$ chains and cationic ligands. The charged inorganic and organic motifs are further connected by either Cu-N or Cu-S coordinate bonds. While the ionic bonds enhance their thermostability and solution-processability, the coordinate bonds play an important role in their (M+X)LCT emission process and optical tunability. The ligands are designed to contain cationic centers (quaternary N atoms) and coordination active sites for subsequent Cu-N or Cu-S bond formation. The molecular structures of organic ligands are shown in Fig. 1 and Figs. S1-S3; along with ^{1}H NMR data to confirm their purity.

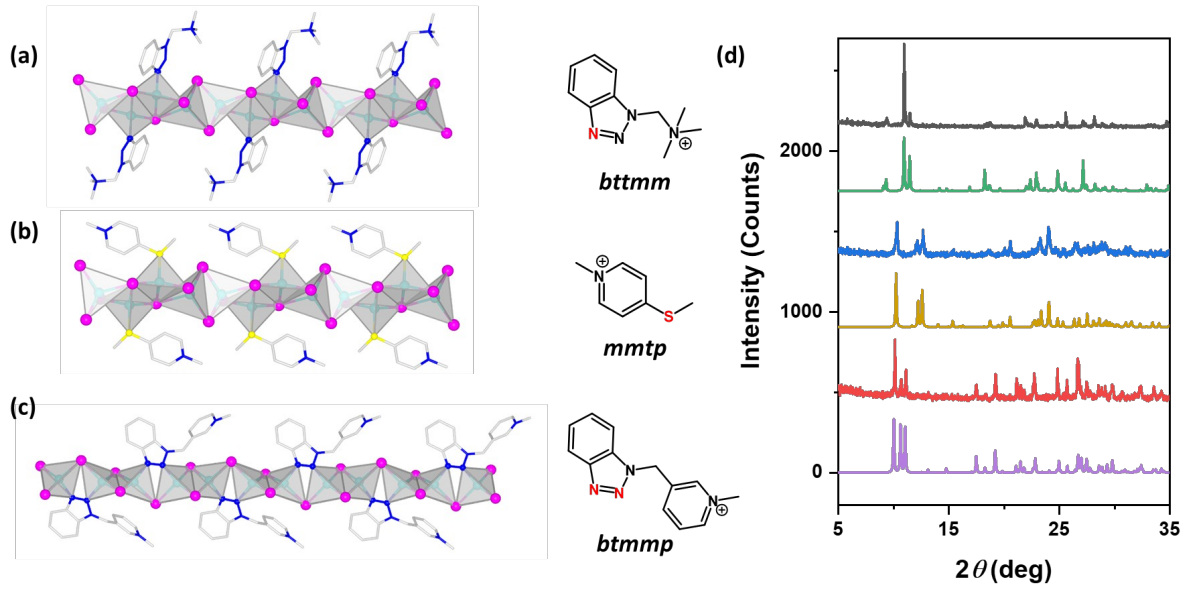

Figure 1. Crystal structures of the title compounds and corresponding ligand structures, (a) **1**, (b) **2**, and (c) **3**. Color scheme: cyan: Cu; purple: I; gray: C; blue: N, yellow: S. All H atoms and disorders are omitted for clarity. Active coordination sites of the ligands are marked in red. (d) PXRD patterns of compounds **1**-**3**. From bottom to top: simulated **1**, as made **1**; simulated **2**, as made **2**; simulated **3** and as made **3**.

The layered diffusion method has proven to be efficient for obtaining high-quality single crystals of CuI-based hybrid structures.[34] Single crystals of all three compounds were obtained by this method, using acetonitrile as a buffer layer to slow the nucleation rate. Crystal images can be found in Fig. S5. The single-crystal X-ray analysis revealed that these compounds share a common formula of $Cu_4I_6(L)_2$, where L is ligand. The 1D anionic inorganic chains within the structure are charge balanced by the cationic ligands that also form coordinative bonds with Cu atoms, as shown in Figs. 1a-c. Important crystallographic data are summarized in Table 1. In all structures, copper atoms are tetrahedrally coordinated to either three iodine and one ligand, or four iodine atoms, while the coordination numbers of iodine atoms range from 2 to 3, similar to the previous reported AIO structures.[4, 7, 22, 30-

32, 35] Despite all anionic chains having the same composition, namely $Cu_4I_6^{2-}$, two different types of chains are observed. In the first type, each ligand is coordinated to only one Cu atom, giving monocoordinated (μ^1-MC) structure. Compounds **1** and **2** adopt this type (Fig. 1a-b). For the second type, each ligand is coordinated to two adjacent Cu atoms, forming a five-membered ring with one bridging I atom (Fig. 1c). This is also noted as a dicoordination (μ^2-DC) structure. Such structural differences are mainly due to the coordination ability of the ligand, which can be predicted and tuned by changing the electron density of the coordination available atoms via inductive effect.[4, 32] The Cu-N and Cu-S bond lengths in these structures are 2.0-2.1 Å and 2.4 Å, respectively, similar to those of Type I structures containing only dative bonds.[36-38]

Table 1. Crystal structure data for **1**–**3**.

	1D-Cu_4I_6(*bttmm*)$_2$ **(1)**	1D-Cu_4I_6(*mmtp*)$_2$ **(2)**	1D-Cu_4I_6(*btmmp*)$_2$ **(3)**
Empirical formula	$C_{10}H_{15}Cu_2I_3N_4$	$C_7H_{10}Cu_2I_3NS$	$C_{13}H_{13}Cu_2I_3N_4$
M_r	699.04	648.00	733.05
Space group	Triclinic, *P*-1	Triclinic, *P*-1	Monoclinic, $P2_1/c$
a, Å	9.2349(4)	7.8476(3)	9.5419(3)
b, Å	9.8411(4)	9.6097(4)	15.4282(4)
c, Å	10.4688(4)	10.2249(4)	12.5930(4)
α, deg	82.882(2)	103.287(2)	90
β, deg	85.189(2)	93.300(2)	96.718(2)
γ, deg	64.311(2)	110.978(2)	90
V, Å^3	850.29(6)	692.36(5)	1841.14(10)
Z	2	2	4
D_{calcd}, g cm^{-3}	2.730	3.108	2.645
μ(MoK_α), mm^{-1}	7.228	12.375	7.788
F(000), e	640	584	1344
hkl range	±15, ±16, ±17	±13, ±16, ±17	±14, ±23, ±18
θ range , deg	$2.468 \le \theta \le 35.070$	$2.258 \le \theta \le 42.936$	$2.150 \le \theta \le 34.138$

Refl. measured	8258	6941	7024
Refl. unique	7906	5668	6378
R_{int}	0.0227	0.0226	0.0530
Param. refined	175	129	201
$R(F)$ / $wR(F^2)$[a] ($I >$ 2 σ(I))	0.0170 / 0.0402	0.0281 / 0.0567	0.0244 / 0.0635
$R(F)$ / $wR(F^2)$[a] (all data)	0.0182 / 0.0406	0.0408 / 0.0610	0.0270 / 0.0652
GoF (F^2)[b]	1.206	1.069	1.084
$\Delta\rho_{fin}$ (max / min), e Å^{-3}	0.628 / -2.264	0.986 / -1.546	1.454 / -1.574

[a] $R(F) = \||F_o|-|F_c|\|/\Sigma|F_o|$, $wR(F^2) = [\Sigma w(F_o^2-F_c^2)^2/\Sigma w(F_o^2)^2]^{1/2}$, $w = [\sigma^2(F_o^2)+(AP)^2+BP]^{-1}$, where $P = (\mathrm{Max}(F_o^2, 0)+2F_c^2)/3$; [b] GoF = $[\Sigma w(F_o^2-F_c^2)^2/(n_{obs}-n_{param})]^{1/2}$

The photophysical properties of all three title compounds were investigated using PL spectroscopy and UV-Vis absorption spectroscopy at room temperature. The important photophysical properties are summarized in Table 2. All three compounds emit low energy lights at wavelengths between 530 and 590 nm, and the emission color ranges from green with Commission International del'Eclairage (CIE) color coordinates (x, y) of (0.37, 0.56) to orange with CIE color coordinates of (0.48, 0.51) (Figs. 2a-c). All compounds can be excited with blue light (450 nm), an important requirement for phosphors that can be used in current commercial WLED devices with blue LED chips.[39, 40] A single band feature was observed for all compounds, with an average full-width at half-maximum (FWHM) of ~100 nm, which has been observed for many CuX-based hybrid materials.[41, 42] The internal quantum yields (IQYs) of all three compounds were determined at room temperature under 360 nm excitation, and are listed in Table 2. The optical bandgaps of the compounds range from 2.3 to 2.6 eV, estimated from their absorption edges as shown in Fig. 2d. The compounds exhibit strong absorption suggesting that they are efficient energy absorbers, ideal for phosphors.

Compound	Bandgap (eV)	λ_{em} (nm)	CIE	IQY [a] (%)	T_d [b] (°C)	Solubility [c] (mg/ml)
$Cu_4I_6(bttmm)_2$ **(1)**	2.6	530	(0.37, 0.56)	41	210	200
$Cu_4I_6(mmtp)_2$ **(2)**	2.4	550	(0.46, 0.52)	21	215	140
$Cu_4I_6(btmmp)_2$ **(3)**	2.5	590	(0.48, 0.47)	52	240	90

Table 2. Summary of important physical properties of compounds **1**-**3**.

[a] λ_{ex} = 360 nm; [b] T_d: Decomposition temperature; [c] Tested in DMSO at room temperature.

Figure 2. (a) Normalized PL excitation spectra. (b) Normalized PL emission spectra; (c) Color chromaticity. (d) Optical absorption spectra. (e) TG plots of compounds **1-3**. Color

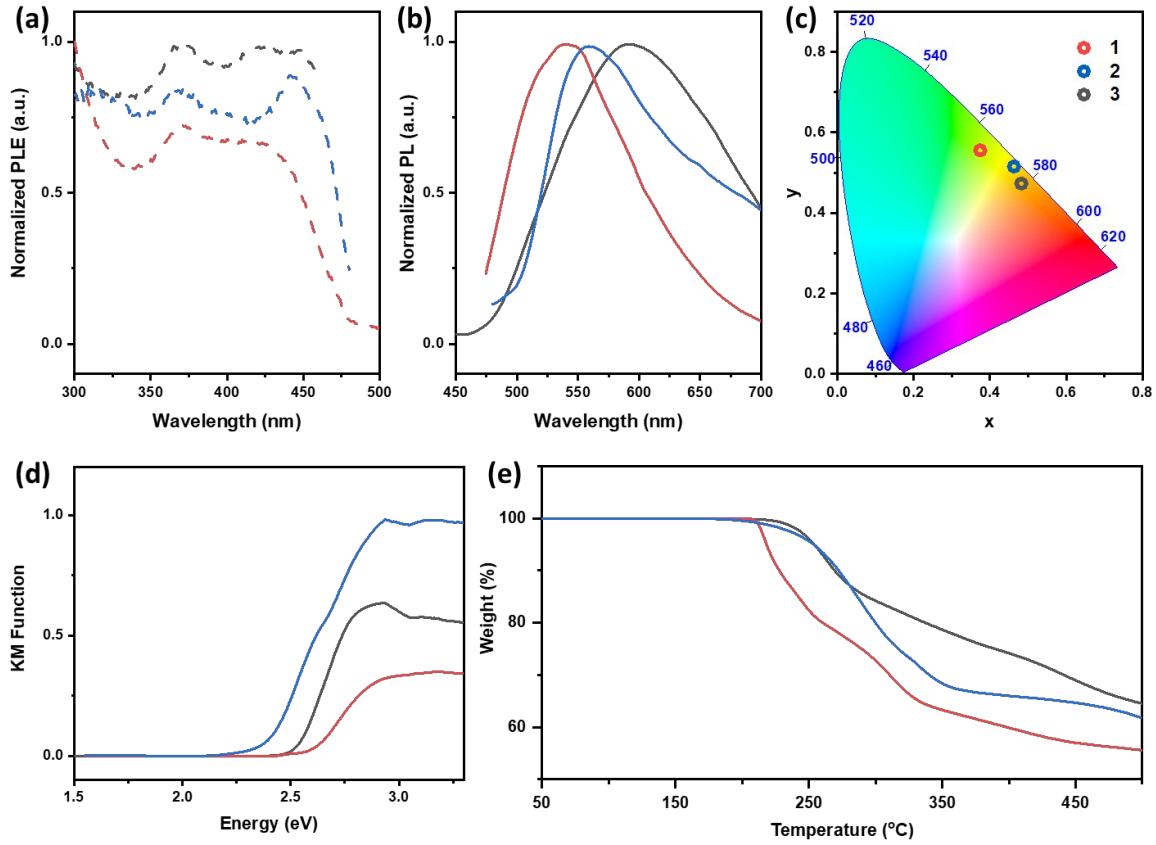

scheme: Red: **1**; Blue: **2** and Black: **3**. All emission spectra were measured at an excitation wavelength of 360 nm and the excitation spectra were collected at the wavelength of their emission maximum.

Thermogravimetric analysis (TGA) was performed to evaluate their thermal stability. All compounds remain stable up to at least 210 °C (Fig. 2e). Based on the previous studies of the thermal decomposition behavior of ionic CuX hybrid structures,[43, 44] the weight losses of 48% (210-550 °C) for **1**, 38% (215-500 °C) for **2** and 42% (240-550 °C) for **3** can be attributed to the loss of [*bttmm*]I (calc. 45%), [*mmtp*]I (calc. 41%) and [*btmmp*]I (calc. 48%), respectively. Compared to charge-neutral 1D-CuI(L) structures which generally decompose below 150 °C,[19, 45] the AIO-type compounds are much more robust, as a result of having both coordinate and ionic bonds between the organic and inorganic components. Such a stability enhancement was also observed in other CuX-based AIO-type hybrid structures reported previously.[4, 23, 35] In addition, it has been proven that with higher connectivity, the ligands can form stronger bonds with the inorganic motifs, yielding hybrids with high thermal resistance.[35, 46] Therefore, with a μ^2-DC binding mode, compound **3** demonstrates a higher decompostion temperature than both compounds **1** and **2** with μ^1-MC binding mode.

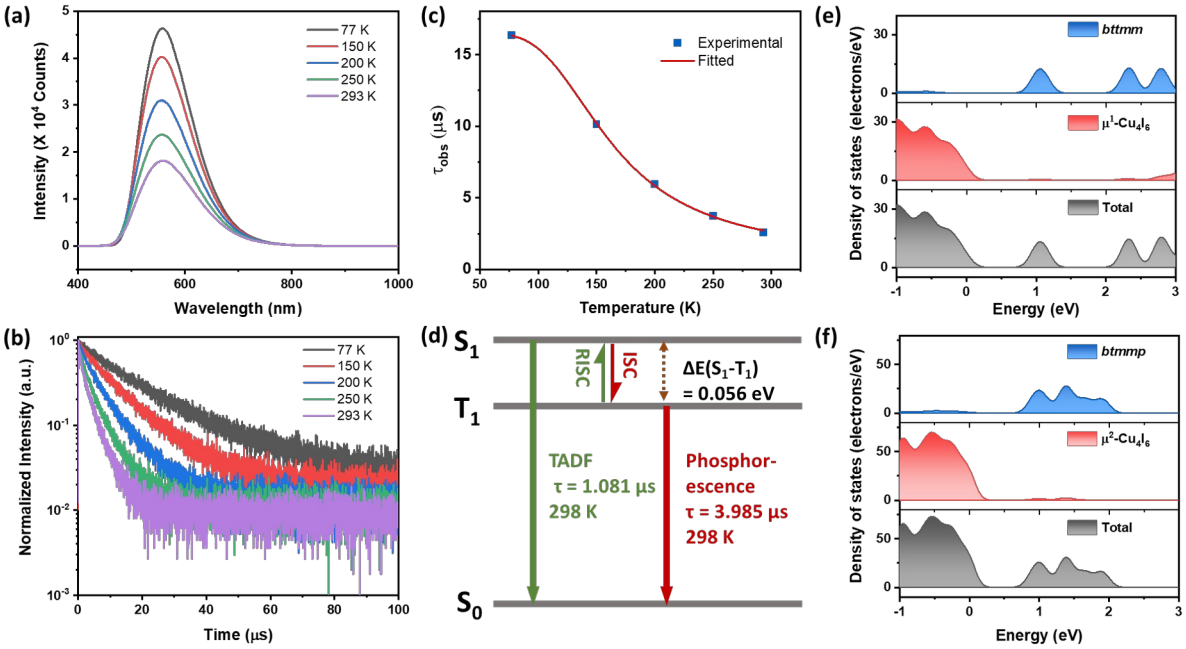

Figure 3. (a) PL emission spectra of compound **1** at various temperature (λ_{em} = 380 nm). (b) Temperature dependent luminescence decay curves of compound **1**. (c) The observed decay times of compound **1** (blue dots) and the fitting curve (red line) according to equation (1). (d) Energy diagram of compound **1** indicating TADF and phosphorescence. (e) and (f) Calculated total density of states (DOS) and projected density of states (PDOS) of compounds **1** and **3**, respectively.

To gain insight into the emission mechanisms, compound **1** was selected to perform temperature dependent PL spectrosscopy and lifetime measurements. The PL lifetime of compound **1** exhibits strong temperature dependence, as its average amplitude-weighted lifetime decreased from ~16 μs at 77 K to ~3 μs at 298 K (Table S1). All the PL lifetime decay curves at various temperatures are best fitted using a biexponential function, indicating two different decay pathways are involved in its emission process. Upon increasing temperature, the fraction of short lifetime decay rises from 19% (5.76 μs) at 77 K to 48% (1.08 μs) at 293 K, while the fraction of longer lifetime decay decreases from 81% (18.81 μs)

at 77 K to 52% (3.99 μs) at 298 K. These data reveal the fact that besides the phosphorescence (emission of longer lifetime), thermally activited delayed fluorescence (TADF, emission of shorter lifetime)) also plays an important role in the emission of these compounds. This phenomenon has been observed in many other previously reported Cu-based inorganic-organic hybrid materials[30, 32, 47] and small organic molecules.[48, 49] TADF often occurs in compounds with small energy differences between the lowest excited singlet state (S_1) and the lowest excited triplet state (T_1). With the thermal energy provided by the envioronment, a fraction of electrons can undergo reverse intersystem crossing (RISC) from T_1 back to S_1, and then follow a radiative transition from S_1 to S_0 as TADF process. The correlation between the observed decay time (τ_{obs}) and absolute temperature (T) can be given as follows according to the literature:[49, 50]

$$\tau_{obs} = \frac{3 + e^{\frac{-\Delta E(S_1 - T_1)}{k_B T}}}{\frac{3}{\tau(T_1)} + \frac{1}{\tau(S_1)} \times e^{\frac{-\Delta E(S_1 - T_1)}{k_B T}}}$$

where k_B is the Boltzmann constant, $\tau(T_1)$ and $\tau(S_1)$ are the decay times of T_1 and S_1 states respectively, and ΔE (S_1-T_1) is the energy difference between the two states. As shown in Fig. 3c, an excellent fit for the observed decay time of compound **1** is obtained. The fitted $\tau(T_1)$ value is 16 μs, similar to the experimental data of 19 μs at 77 K, comfirming the good fitting. The ΔE (S_1-T_1) of compound **1** was estimated to be 0.056 eV, similar to that of other reported compounds exhibiting efficient TADF process.[42, 49, 51] Such small energy splitting is essential to boost the efficient TADF at ambient temperatures. In addition, only very small blue shift of the emission spectra of compound **1** was observed by increasing temperature from 77 K to 298 K, which can be attributed to the indistinguishishable energy of S_1 and T_1.

Density functional theory (DFT) calculations were conducted to calculate the projected density of states (PDOS) for all three compounds using the Cambridge Serial Total Energy Package (CASTEP) in Material Studio.[52] As shown in Fig. 3e-f and Figs. S6-S8, all compounds share similar features. The atomic states that contribute to the valence band maximum (VBM) are mostly from inorganic components (Cu 3d and I 5p orbitals), while the atomic states in the conduction band minimum (CBM) are primarily from the organic component (C 2p, N 2p and/or S 3p orbitals). This indicates the fact that the emission mechanism of all three compounds can be attributed to a combination of metal-to-ligand charge transfer (MLCT) and halide-to-ligand charge transfer (XLCT), or (M+X)LCT. Compared to the rare-earth element containing commercial phosphors, whose emissions come from the atomic orbitals of Ce^{3+} or Eu^{3+},[53, 54] the AIO-type hybrid materials demonstrate a much larger extent of bandgap tunability and their emission c matically altered by using ligands with desired lowest unoccupied molecu energies. The calculated bandgaps of all three compounds are well in t erimental optical bandgap values, but have relatively smaller values. Th lculation used generalized gradient approximation (GGA) functional, which is well known to underestimate the bandgaps.[55]

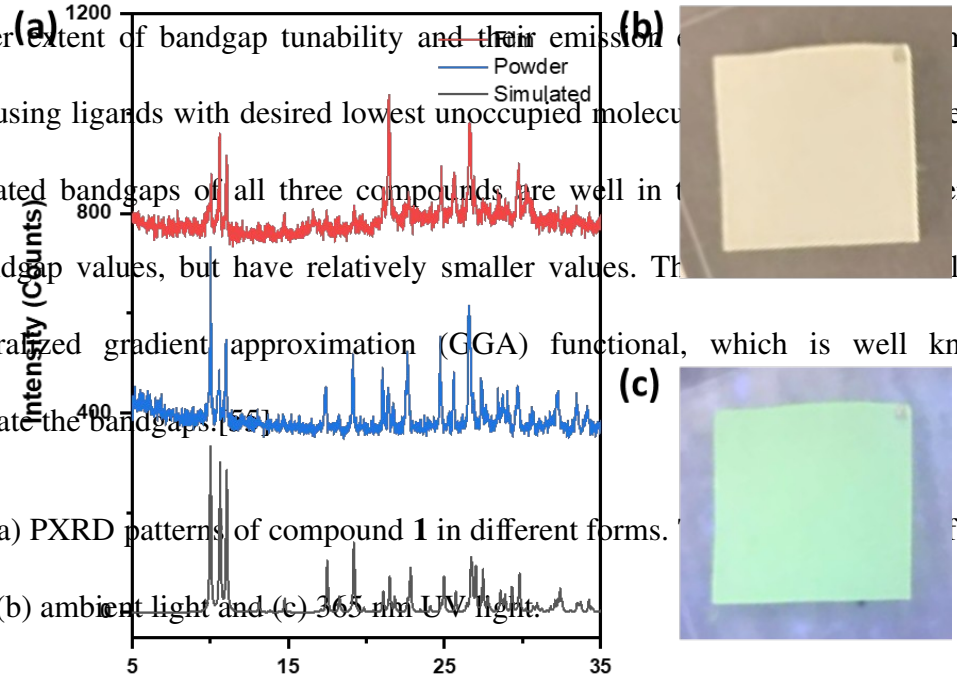

Figure 4. (a) PXRD patterns of compound **1** in different forms. f the thin film under (b) ambient light and (c) 365 nm UV light.

Another important advantage of AIO compounds lies in their solution-processability. It is well recognized that solution-processed semiconductors have become a new paradigm in optoelectronic device industries.[56, 57] Compared to the conventional inorganic semiconductors which require high cost for device manufacture, solution-processible

materials have the distinct advantage because high-quality thin films can be fabricated by simple and cost-effective methods, including spin coating, blade coating, inkjet printing and other existing printing technologies.[58, 59] All title compounds exhibit outstanding solubility in polar aprotic solvents such as DMSO, despite the extended nature of their 1D inorganic chains, while most of the Type I CuI-based extended structures (1D-3D) show very poor solubility in any common solvents.[10, 36, 37] Previous studies on the solvation behavior of the AIO-type compounds have suggested that this intriguing phenomenon is a result of introducing ionic bonds between the inorganic and organic motifs.[4, 32, 35] As a preliminary test, we prepared thin film samples of the AIO compounds by direct drop-casting of the AIO/ DMSO solutions on glass substrates (Fig. 4a, c). After annealing at 110 °C for 30 min, both the crystallinity and luminescence of the film samples were restored. As shown in Fig. 4b, the PXRD pattern of the film sample matches well with that of the powder sample. The PL spectrum of the film sample remains nearly identical to that of the polycrystalline sample, with a slight peak broadening (Fig. S9).

Conclusion

In summary, three new AIO-type organic-inorganic hybrid materials made of 1D-$Cu_4I_6^{2-}$ anionic chains and cationic ligands were synthesized. Two different types of inorganic chains and ligand coordination modes were identified. All compounds remain stable up to at least 210 °C. They emit green to orange colors (530-590 nm) under UV (360 nm) irradiation and can be well excited by blue light (450 nm). The emission mechanism was studied both experimentally and theoretically. All three compounds exhibit remarkable solution processability due to their unique bonding nature, as a result of introducing ionic bonds between the inorganic and organic motifs.

Acknowledgments

The authors acknowledge the partial support from the U.S. Department of Energy, Office of Science, Office of Basic Energy Sciences (Grant No. DE-SC0019902). This research used the Advanced Light Source (ALS), which is a DOE Office of Science User Facility under contract No. DE-AC02-05CH11231. The temperature dependent luminescence work was carried out at the Center for Functional Nanomaterials, Brookhaven National Laboratory (BNL), which is supported by the U.S. Department of Energy, Office of Basic Energy Sciences, under Contract No. DE-SC0012704.

References

[1] B. Saparov, D.B. Mitzi, Organic–Inorganic Perovskites: Structural Versatility for Functional Materials Design, Chem. Rev. 116(7) (2016) 4558-4596.
[2] V.W.-W. Yam, V.K.-M. Au, S.Y.-L. Leung, Light-Emitting Self-Assembled Materials Based on d^8 and d^{10} Transition Metal Complexes, Chem. Rev. 115(15) (2015) 7589-7728.
[3] M. Li, Z. Xia, Recent progress of zero-dimensional luminescent metal halides, Chem. Soc. Rev. 50(4) (2021) 2626-2662.
[4] X. Hei, J. Li, All-in-one: a new approach toward robust and solution-processable copper halide hybrid semiconductors by integrating covalent, coordinate and ionic bonds in their structures, Chem. Sci. 12(11) (2021) 3805-3817.
[5] N.J. Jeon, J.H. Noh, W.S. Yang, Y.C. Kim, S. Ryu, J. Seo, S.I. Seok, Compositional engineering of perovskite materials for high-performance solar cells, Nature 517(7535) (2015) 476-480.
[6] M.D. Smith, H.I. Karunadasa, White-Light Emission from Layered Halide Perovskites, Acc. Chem. Res. 51(3) (2018) 619-627.
[7] K. Zhu, Z. Cheng, S. Rangan, M. Cotlet, J. Du, L. Kasaei, S.J. Teat, W. Liu, Y. Chen, L.C. Feldman, D.M. O'Carroll, J. Li, A New Type of Hybrid Copper Iodide as Nontoxic and Ultrastable LED Emissive Layer Material, ACS Energy Lett. 6(7) (2021) 2565-2574.
[8] H. Huang, B. Pradhan, J. Hofkens, M.B.J. Roeffaers, J.A. Steele, Solar-Driven Metal Halide Perovskite Photocatalysis: Design, Stability, and Performance, ACS Energy Lett. 5(4) (2020) 1107-1123.
[9] X.-W. Lei, C.-Y. Yue, J.-Q. Zhao, Y.-F. Han, J.-T. Yang, R.-R. Meng, C.-S. Gao, H. Ding, C.-Y. Wang, W.-D. Chen, Low-Dimensional Hybrid Cuprous Halides Directed by Transition Metal Complex: Syntheses, Crystal Structures, and Photocatalytic Properties, Cryst. Growth Des. 15(11) (2015) 5416-5426.
[10] F. Deschler, M. Price, S. Pathak, L.E. Klintberg, D.-D. Jarausch, R. Higler, S. Hüttner, T. Leijtens, S.D. Stranks, H.J. Snaith, M. Atatüre, R.T. Phillips, R.H. Friend, High Photoluminescence Efficiency and Optically Pumped Lasing in Solution-Processed Mixed Halide Perovskite Semiconductors, J. Phys. Chem. Lett. 5(8) (2014) 1421-1426.
[11] V. Kovalenko Maksym, L. Protesescu, I. Bodnarchuk Maryna, Properties and potential optoelectronic applications of lead halide perovskite nanocrystals, Science 358(6364) (2017) 745-750.
[12] R. Peng, M. Li, D. Li, Copper(I) halides: A versatile family in coordination chemistry and crystal engineering, Coord. Chem. Rev. 254(1) (2010) 1-18.
[13] W. Liu, W.P. Lustig, J. Li, Luminescent inorganic-organic hybrid semiconductor materials for energy-saving lighting applications, EnergyChem 1(2) (2019) 100008.
[14] J. Yan, B.K. Teo, N. Zheng, Surface Chemistry of Atomically Precise Coinage–Metal Nanoclusters: From Structural Control to Surface Reactivity and Catalysis, Acc. Chem. Res. 51(12) (2018) 3084-3093.
[15] L. Mao, P. Guo, S. Wang, A.K. Cheetham, R. Seshadri, Design Principles for Enhancing Photoluminescence Quantum Yield in Hybrid Manganese Bromides, J. Am. Chem. Soc. 142(31) (2020) 13582-13589.
[16] K. Tsuge, Y. Chishina, H. Hashiguchi, Y. Sasaki, M. Kato, S. Ishizaka, N. Kitamura, Luminescent copper(I) complexes with halogenido-bridged dimeric core, Coord. Chem. Rev. 306 (2016) 636-651.

[17] E. Cariati, E. Lucenti, C. Botta, U. Giovanella, D. Marinotto, S. Righetto, Cu(I) hybrid inorganic–organic materials with intriguing stimuli responsive and optoelectronic properties, Coord. Chem. Rev. 306 (2016) 566-614.
[18] X. Feng, C. Xu, Z.-Q. Wang, S.-F. Tang, W.-J. Fu, B.-M. Ji, L.-Y. Wang, Aerobic Oxidation of Alcohols and the Synthesis of Benzoxazoles Catalyzed by a Cuprocupric Coordination Polymer (Cu^{+}-CP) Assisted by TEMPO, Inorg. Chem. 54(5) (2015) 2088-2090.
[19] X. Zhang, W. Liu, G.Z. Wei, D. Banerjee, Z. Hu, J. Li, Systematic Approach in Designing Rare-Earth-Free Hybrid Semiconductor Phosphors for General Lighting Applications, J. Am. Chem. Soc. 136(40) (2014) 14230-14236.
[20] Y. Fang, C.A. Sojdak, G. Dey, S.J. Teat, M. Li, M. Cotlet, K. Zhu, W. Liu, L. Wang, D.M. ÓCarroll, J. Li, Highly efficient and very robust blue-excitable yellow phosphors built on multiple-stranded one-dimensional inorganic–organic hybrid chains, Chem. Sci. 10(20) (2019) 5363-5372.
[21] C. Chen, R.-H. Li, B.-S. Zhu, K.-H. Wang, J.-S. Yao, Y.-C. Yin, M.-M. Yao, H.-B. Yao, S.-H. Yu, Highly Luminescent Inks: Aggregation-Induced Emission of Copper–Iodine Hybrid Clusters, Angew. Chem. Int. Ed. 57(24) (2018) 7106-7110.
[22] A.V. Artem'ev, M.P. Davydova, X. Hei, M.I. Rakhmanova, D.G. Samsonenko, I.Y. Bagryanskaya, K.A. Brylev, V.P. Fedin, J.-S. Chen, M. Cotlet, J. Li, Family of Robust and Strongly Luminescent CuI-Based Hybrid Networks Made of Ionic and Dative Bonds, Chem. Mater. 32(24) (2020) 10708-10718.
[23] W. Liu, Y. Fang, J. Li, Copper Iodide Based Hybrid Phosphors for Energy-Efficient General Lighting Technologies, Adv. Funct. Mater. 28(8) (2018) 1705593.
[24] J.-S. Yao, J.-J. Wang, J.-N. Yang, H.-B. Yao, Modulation of Metal Halide Structural Units for Light Emission, Acc. Chem. Res. 54(2) (2021) 441-451.
[25] W. Ki, X. Hei, H.T. Yi, W. Liu, S.J. Teat, M. Li, Y. Fang, V. Podzorov, E. Garfunkel, J. Li, Two-Dimensional Copper Iodide-Based Inorganic–Organic Hybrid Semiconductors: Synthesis, Structures, and Optical and Transport Properties, Chem. Mater. 33(13) (2021) 5317-5325.
[26] J. Troyano, F. Zamora, S. Delgado, Copper(I)–iodide cluster structures as functional and processable platform materials, Chem. Soc. Rev. 50(7) (2021) 4606-4628.
[27] S.-L. Li, F.-Q. Zhang, X.-M. Zhang, An organic-ligand-free thermochromic luminescent cuprous iodide trinuclear cluster: evidence for cluster centered emission and configuration distortion with temperature, Chem. Commun. 51(38) (2015) 8062-8065.
[28] T.-L. Yu, Y.-M. Guo, G.-X. Wu, X.-F. Yang, M. Xue, Y.-L. Fu, M.-S. Wang, Recent progress of d^{10} iodoargentate(I)/iodocuprate(I) hybrids: Structural diversity, directed synthesis, and photochromic/thermochromic properties, Coord. Chem. Rev. 397 (2019) 91-111.
[29] S. Chen, J. Gao, J. Chang, Y. Li, C. Huangfu, H. Meng, Y. Wang, G. Xia, L. Feng, Family of Highly Luminescent Pure Ionic Copper(I) Bromide Based Hybrid Materials, ACS Appl. Mater. Interfaces 11(19) (2019) 17513-17520.
[30] W. Liu, K. Zhu, S.J. Teat, G. Dey, Z. Shen, L. Wang, D.M. O'Carroll, J. Li, All-in-One: Achieving Robust, Strongly Luminescent and Highly Dispersible Hybrid Materials by Combining Ionic and Coordinate Bonds in Molecular Crystals, J. Am. Chem. Soc. 139(27) (2017) 9281-9290.
[31] X. Hei, S.J. Teat, W. Liu, J. Li, Eco-friendly, solution-processable and efficient low-energy lighting phosphors: copper halide based hybrid semiconductors $Cu_4X_6(L)_2$ (X = Br, I) composed of covalent, ionic and coordinate bonds, J. Mater. Chem. C 8(47) (2020) 16790-16797.

[32] X. Hei, W. Liu, K. Zhu, S.J. Teat, S. Jensen, M. Li, D.M. O'Carroll, K. Wei, K. Tan, M. Cotlet, T. Thonhauser, J. Li, Blending Ionic and Coordinate Bonds in Hybrid Semiconductor Materials: A General Approach toward Robust and Solution-Processable Covalent/Coordinate Network Structures, J. Am. Chem. Soc. 142(9) (2020) 4242-4253.
[33] G. Sheldrick, Crystal structure refinement with SHELXL, Acta Crystallogr. C 71(1) (2015) 3-8.
[34] X. Hei, Y. Fang, S.J. Teat, C. Farrington, M. Bonite, J. Li, Copper(I) iodide-based organic–inorganic hybrid compounds as phosphor materials, Z. Naturforsch. B 76(10-12) (2021) 759-764.
[35] A.V. Artem'ev, E.A. Pritchina, M.I. Rakhmanova, N.P. Gritsan, I.Y. Bagryanskaya, S.F. Malysheva, N.A. Belogorlova, Alkyl-dependent self-assembly of the first red-emitting zwitterionic $\{Cu_4I_6\}$ clusters from [alkyl-P(2-Py)$_3$]$^+$ salts and CuI: when size matters, Dalton Trans. 48(7) (2019) 2328-2337.
[36] Y. Fang, W. Liu, S.J. Teat, G. Dey, Z. Shen, L. An, D. Yu, L. Wang, D.M. O'Carroll, J. Li, A Systematic Approach to Achieving High Performance Hybrid Lighting Phosphors with Excellent Thermal- and Photostability, Adv. Funct. Mater. 27(3) (2017) 1603444.
[37] W. Liu, Y. Fang, G.Z. Wei, S.J. Teat, K. Xiong, Z. Hu, W.P. Lustig, J. Li, A Family of Highly Efficient CuI-Based Lighting Phosphors Prepared by a Systematic, Bottom-up Synthetic Approach, J. Am. Chem. Soc. 137(29) (2015) 9400-9408.
[38] T.S. Lobana, Rekha, R.J. Butcher, A. Castineiras, E. Bermejo, P.V. Bharatam, Bonding Trends of Thiosemicarbazones in Mononuclear and Dinuclear Copper(I) Complexes: Syntheses, Structures, and Theoretical Aspects, Inorg. Chem. 45(4) (2006) 1535-1542.
[39] X. Huang, Red phosphor converts white LEDs, Nat. Photonics 8(10) (2014) 748-749.
[40] P. Pust, V. Weiler, C. Hecht, A. Tücks, A.S. Wochnik, A.-K. Henß, D. Wiechert, C. Scheu, P.J. Schmidt, W. Schnick, Narrow-band red-emitting Sr[$LiAl_3N_4$]:Eu^{2+} as a next-generation LED-phosphor material, Nat. Mater. 13(9) (2014) 891-896.
[41] Y.Y. Liu, X. Zhang, K. Li, Q.C. Peng, Y.J. Qin, H.W. Hou, S.Q. Zang, B.Z. Tang, Restriction of Intramolecular Vibration in Aggregation-Induced Emission Luminogens: Applications in Multifunctional Luminescent Metal–Organic Frameworks, Angew. Chem. Int. Ed. 60(41) (2021) 22417-22423.
[42] H. Li, Y. Lv, Z. Zhou, H. Tong, W. Liu, G. Ouyang, Coordinated Anionic Inorganic Module—An Efficient Approach Towards Highly Efficient Blue-Emitting Copper Halide Ionic Hybrid Structures, Angew. Chem. Int. Ed. 61(8) (2022) e202115225.
[43] P. Hao, Y. Qiao, T. Yu, J. Shen, F. Liu, Y. Fu, Three iodocuprate hybrids symmetrically modulated by positional isomers and the chiral conformation of N-benzyl-methylpyridinium, RSC Adv. 6(58) (2016) 53566-53572.
[44] J.-J. Shen, X.-X. Li, T.-L. Yu, F. Wang, P.-F. Hao, Y.-L. Fu, Ultrasensitive Photochromic Iodocuprate(I) Hybrid, Inorg. Chem. 55(17) (2016) 8271-8273.
[45] W. Liu, D. Banerjee, F. Lin, J. Li, Strongly luminescent inorganic–organic hybrid semiconductors with tunable white light emissions by doping, J. Mater. Chem. C 7(6) (2019) 1484-1490.
[46] G. Schwarzenbach, Der Chelateffekt, Helv. Chim. Acta 35(7) (1952) 2344-2359.
[47] T. Hofbeck, U. Monkowius, H. Yersin, Highly Efficient Luminescence of Cu(I) Compounds: Thermally Activated Delayed Fluorescence Combined with Short-Lived Phosphorescence, J. Am. Chem. Soc. 137(1) (2015) 399-404.
[48] M. Li, Y.-F. Wang, D. Zhang, L. Duan, C.-F. Chen, Axially Chiral TADF-Active Enantiomers Designed for Efficient Blue Circularly Polarized Electroluminescence, Angew. Chem. Int. Ed. 59(9) (2020) 3500-3504.

[49] R. Hamze, L. Peltier Jesse, D. Sylvinson, M. Jung, J. Cardenas, R. Haiges, M. Soleilhavoup, R. Jazzar, I. Djurovich Peter, G. Bertrand, E. Thompson Mark, Eliminating nonradiative decay in Cu(I) emitters: >99% quantum efficiency and microsecond lifetime, Science 363(6427) (2019) 601-606.
[50] R. Czerwieniec, J. Yu, H. Yersin, Blue-Light Emission of Cu(I) Complexes and Singlet Harvesting, Inorg. Chem. 50(17) (2011) 8293-8301.
[51] M.J. Leitl, V.A. Krylova, P.I. Djurovich, M.E. Thompson, H. Yersin, Phosphorescence versus Thermally Activated Delayed Fluorescence. Controlling Singlet–Triplet Splitting in Brightly Emitting and Sublimable Cu(I) Compounds, J. Am. Chem. Soc. 136(45) (2014) 16032-16038.
[52] S.J. Clark, M.D. Segall, C.J. Pickard, P.J. Hasnip, M.I.J. Probert, K. Refson, M.C. Payne, First principles methods using CASTEP, Z. Kristallogr. Cryst. Mater. 220(5-6) (2005) 567-570.
[53] L. Chen, C.-C. Lin, C.-W. Yeh, R.-S. Liu, Light Converting Inorganic Phosphors for White Light-Emitting Diodes, Materials 3(3) (2010).
[54] S. Ye, F. Xiao, Y.X. Pan, Y.Y. Ma, Q.Y. Zhang, Phosphors in phosphor-converted white light-emitting diodes: Recent advances in materials, techniques and properties, Mater. Sci. Eng. R Rep. 71(1) (2010) 1-34.
[55] J. Muscat, A. Wander, N.M. Harrison, On the prediction of band gaps from hybrid functional theory, Chem. Phys. Lett. 342(3) (2001) 397-401.
[56] W. Nie, H. Tsai, R. Asadpour, J.-C. Blancon, J. Neukirch Amanda, G. Gupta, J. Crochet Jared, M. Chhowalla, S. Tretiak, A. Alam Muhammad, H.-L. Wang, D. Mohite Aditya, High-efficiency solution-processed perovskite solar cells with millimeter-scale grains, Science 347(6221) (2015) 522-525.
[57] K. Lin, J. Xing, L.N. Quan, F.P.G. de Arquer, X. Gong, J. Lu, L. Xie, W. Zhao, D. Zhang, C. Yan, W. Li, X. Liu, Y. Lu, J. Kirman, E.H. Sargent, Q. Xiong, Z. Wei, Perovskite light-emitting diodes with external quantum efficiency exceeding 20 per cent, Nature 562(7726) (2018) 245-248.
[58] M. Singh, H.M. Haverinen, P. Dhagat, G.E. Jabbour, Inkjet Printing—Process and Its Applications, Adv. Mater. 22(6) (2010) 673-685.
[59] F.C. Krebs, Fabrication and processing of polymer solar cells: A review of printing and coating techniques, Sol. Energy Mater. Sol. Cells 93(4) (2009) 394-412.